

# Current-Fed Quasi Z-Source Inverter based PV Distributed Generation Controller

Faris E. Alfaris  
Student member, IEEE  
*Electrical and Computer Engineering*  
North Carolina State University  
Raleigh, United States  
Fealfari@ncsu.edu

Subhashish Bhattacharya  
Senior member, IEEE  
*Electrical and Computer Engineering*  
North Carolina State University  
Raleigh, United States  
Sbhatta4@ncsu.edu

**Abstract** – Recently, the renewable photovoltaic distributed generation (PV-DG) enjoys a rapid growth globally due to the advancement in solar systems and power electronics technologies. However, the intermittent nature of solar radiation and performance of the attached power converters, inevitably poses some challenges to the power grids integrated large-scale solar-farms (SF). These challenges include frequency oscillations, voltage variation and power quality issues. To overcome these problems, this study proposes a Current-Fed quasi Z-source Inverter (CF-qZSI) as an alternative converter for distribution generation controllers to facilitate the integration of a PV energy source into a weak power system. The detailed model of the CF-qZSI-based distribution controller (CqZDC) and its control system are developed. The dynamic performance of the CqZDC device is evaluated to validate different objectives using an actual field data and RTDS simulation platform.

**Index Terms**—Accommodation of renewable energy resources, current source inverter, facilitating of distributed electricity generations, frequency stability, power quality improving, wide band gap devices.

## I. INTRODUCTION

Thanks to the recent advancement in renewable energy technologies on account of scientific community and industry contributions, Photovoltaic Distributed Generation (PV-DG) is now significantly considered in supplying electricity amidst distribution networks. One limitation on attaching more and more PV sources to supply higher percentage of the total power demand, is the power quality issues that adversely affected by the penetration and fluctuation in the PV generated power and the negative impact of the attached power converters [1-2]. Additionally, taking a place of the conventional generators by renewable energy sources, results in reducing the overall power system inertia [3-4]. This inertia is favorable for frequency dynamic enhancement, and it becomes not guaranteed due to the detaching of rotating generators that have high kinetic stored energy. This is a gap power conditioning systems (PCS) can fill in. Table I lists the average inertia constant for different generation turbines.

TABLE I. INERTIA CONSTANTS FOR DIFFERENT GENERATION TURBINES [4]

System Turbine	H (s)
Steam	4-9
Gas	3-4
Hydro	2-4
Wind	2-5
Solar PV	0

Based on the aforementioned dynamic considerations on integration of a renewable energy distributed generation, the power system developers must improve the quality of the injected power before authorizing interconnection of PV-DG to distribution feeders. The power quality is an electrical term that describes the ability of the electricity supplies to generate a clean and stable power, and can be measured by different parameters involves voltage, current, frequency and power factor. These parameters must obey to the grid codes and standards that required by the Institute of Electrical and Electronics Engineers (IEEE) to assure desirable power quality. These standards and requirements are as follows:

- 1) Voltage Flicker requirement: The fluctuating nature of power supplied by a PV-DG system can cause of voltage deviations at the grid interfaced bus. These voltage flickers must follow the limits that stated by IEEE-1453 standard.
- 2) Voltage and current Harmonic requirements: Most of the PV systems require interface power converters, which are significant sources of current harmonics. IEEE-519 standard obtains the acceptable range of the current and voltage harmonics at the Point of Interconnection (POI) bus.
- 3) Temporary overvoltage (TOV) requirement: This requirement obeys to IEEE-1547 standard that recommends the TOV limits under normal and unbalanced conditions.
- 4) Power factor requirement: This requirement obey to the Large Generator Interconnection Agreement (LGIA), which necessitates 0.95 power factor at the (POI) bus, calculated at maximum net power [5].
- 5) Online frequency requirement: The sudden disturbances in the supplied or consumed active power causes severe variations in the grid frequency that reduces the power stability, especially for the PV side sub-transmission system. Therefore, the online frequency at the output terminal of the PV-DG must be regulated at nominal value with meeting the frequency dynamic criteria, such as rate of change of frequency (ROCOF) and frequency nadir [4].

In order to meet the aforementioned grid requirements, numerous studies ([6-8]) investigated the impact of the static synchronous compensator (STATCOM) in facilitating the integration of renewable energy sources in order to meet the technical voltage specifications required in grid codes. Including an ESS to STATCOM devices, as in PCS, for the purpose of peak power shaving or power supporting during peak time, is also investigated in [9]. In [10], the utilization of a cascaded multilevel converter based STATCOM, to regulate the voltage at the POI, was validate for integration of a large

scale wind farm into an actual weak power system. The study in [11] proposes a control scheme for PCS constructed of voltage source inverter (VSI) based distributed STATCOM, bi-directional DC-DC chopper converter and vanadium redox flow battery. Recent studies were conducted in [12] and [13] to evaluate sizing and managing of a multi-objective battery energy storage system (BESS) enhancing the integration of a large scale PV system into a medium voltage power plant and residential distribution grid; respectively. These studies also show that facilitating the integration of PV source can contribute in reducing of the overall power loss.

The voltage-fed Z-source and quasi Z-source inverters are tested as a building block for PCS as in [14]. Current source inverters, with simpler output AC filter, are also utilized for PSC in integration of renewable sources as in [15]. High power rating (>10 MVA) converters, such as Cascaded H-bridge converter (CHC) and Modular Multilevel Converter (MMC), are not considered in this study.

Practically, higher power density with continuous bi-directional DC input current is very desirable. Accordingly, most of the inverters topologies discussed in the literature are suffering from different aspects as shown in Table II.

TABLE II. CONSIDERATIONS ON POWER CONVERTERS FOR LOW VOLTAGE-BESS

Converter Type	System considerations
VSI	Requires a DC-DC bi-directional buck/boost converter. A bulky and lossy DC link capacitor is needed. Produces undesirable output voltage waveforms that cause high EMI noise and power loss.
CSI	Unidirectional power flow. High conduction loss. Suited only for boost operation modes.
VF-ZSI	Unidirectional power flow. Discontinuous input current.
CF-ZSI	High stress on passive elements [16]. Ununiformed DC rail.
VF-qZSI	Unidirectional power flow. Ununiformed DC rail.

Therefore, in this study, a recent proposed Current-Fed quasi Z-source Inverter (CF-qZSI) is utilized as an alternative building

block for the PSC versatile device to enhance the power quality of a PV solar farm injected into a distribution network. The CF-qZSI is proposed in [16] with hardware validation. Its efficiency with different aspects in circuit implementation is well obtained in [17]. The capability of buck/boost and bi-directional operations, with single-power stage, makes this inverter an attractive alternative in BESS applications. As the PCS requires a fast response for transition between charging and discharging modes, the study in [18] shows that this transition period takes several switching cycles based on the inverter parameters. From protection point of view, current source inverters offer an advantage of fault protection capabilities, where the input side is in series with current limiter inductors [19]. Distortions in output waveforms can be also reduced, since the overlapping in SVPWM is not required [16].

The detailed model of the power system integrates a 10 MW SF is described in the next section, and the impact of the proposed device is investigated using the Real Time Digital Simulator (RTDS) simulation environment. The field data, collected by supervisory control and data acquisition (SCADA) in [20], are used in the simulation process in order to obtain the capability of the CqZDC in reality. The actual implementation of the controller circuit is planned for future work, and the RTDS simulation tool will be used for controller verification.

## II. CF-QZSI BASED DISTRIBUTION CONTROLLER

### A. Operation Principle and Dynamic Model

The CqZDC is a transportable modular distribution controller which can be connected to distribution voltage bus in order to perform several tasks by conducting the corresponding operation mode. These tasks include the power factor correction, compensating for the current and voltage harmonics to mitigate harmonic distortions at the POI bus, regulating the interface bus voltage to meet utility flicker requirement and supporting the stability of the sub-transmission system that linked the SF to the power grid during PV power fluctuating and load interruptions. The CqZDC consists mainly of a fast-response ESS and bi-directional CF-qZSI as illustrated in Fig. 1. The main objective of the CF-qZSI is to regulate the active and reactive power independently, in charging and discharging modes, in order to achieve the desired functionalities, besides

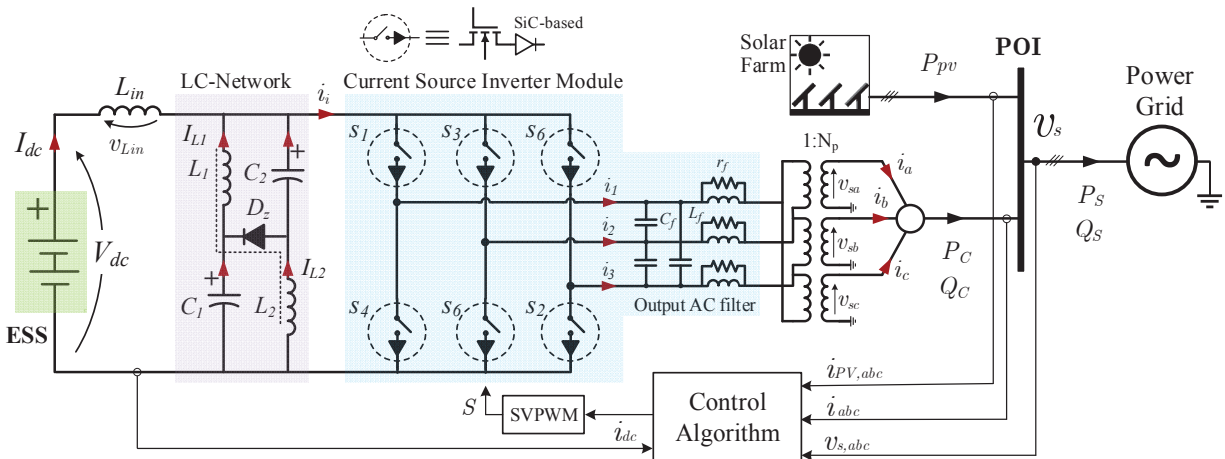


Fig. 1. Configuration of the buck/boost bi-directional CqZDC at the POI bus.

adapting different levels of DC voltage and directing the electric power either to charge or discharge the ESS. The direction of the power flow at the terminal of the power converter is based on the nature of the PV injected power. The step-up delta-wye transformer, placed between the CF-qZSI and the POI bus, is required to reach the grid voltage level and preventing the transferring of the zero-order harmonics from PV side to the power grid. The inverter passive elements are designed to maintain the continuity of the ESS input current with 2% current ripple for all possible operations. The direction of the input LC-network currents during charging and discharging modes are shown in Fig. 2.

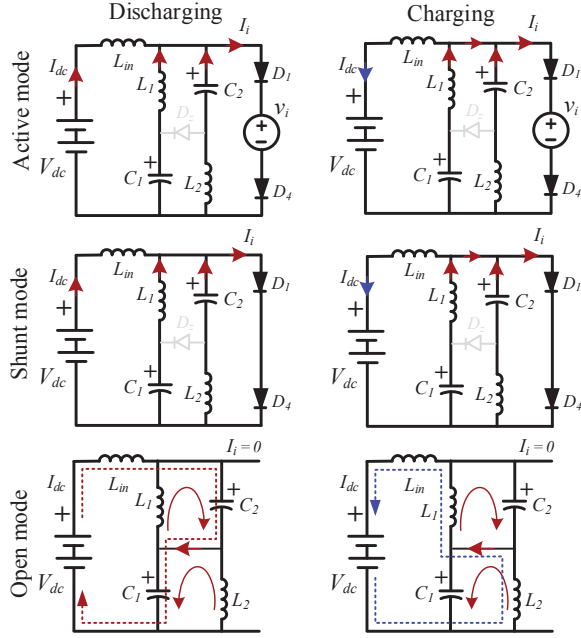


Fig. 2. LC-network currents during charging and discharging modes.

### B. Inverter Design Considerations

The key component of the power inverter is semiconductor switches and system design. Better system performance can be achieved using Si and SiC hybrid semiconductor configuration. In this study, the characteristic of high voltage SiC based MOSFETs and SiC JBS diodes are used to build the power conditioning inverter in sake of higher power rating and higher efficiency [17].

With knowing the input and output voltages and powers, the inverter output peak current can be written by applying the Kirchhoff current law KCL as:

$$\hat{i}_{123} = \left[ \tilde{i}_f + \frac{\tilde{i}_{abc}}{N_p} \right]_{peak} \quad (1)$$

$$= \sqrt{2} \left[ \frac{Q_f}{\sqrt{3} v_f} \angle -90^\circ + \frac{P_o}{N_p \sqrt{3} v_{sab} p f_o} \angle -\cos^{-1}(p f_o) \right] \quad (2)$$

where  $Q_f$ ,  $v_f$  and  $i_f$  are the reactive power, voltage and current for the output filter, respectively.  $p f_o$  is the output power factor.

The well-known relationship between the maximum output current and the PWM modulation index ( $m_i$ ) is:

$$i_{123} = \frac{\sqrt{3}}{2} m_a i_i = \frac{\pi}{3} D_A \{I_{dc} + I_{L1} + I_{L2}\}$$

$$\text{where } I_{L1} = I_{L2} = I_{dc} \left[ \frac{D_{op}}{1 - 2D_{op}} \right] \quad (3)$$

where  $D_A$ ,  $D_{sh}$  and  $D_{op}$  are the duty cycles of the active mode, shunt mode and open mode intervals, respectively. Hence, from (3) and (4), the required short and open duty cycles to draw the desired power from ESS side is:

$$\frac{1 - (D_{sh} + D_{op})}{1 - 2D_{op}} = \frac{3 \hat{i}_{123}}{\pi I_{dc}} \quad (5)$$

$$\gg D_{op} = \frac{\left( \frac{3}{\pi} \hat{i}_{123} I_{dc}^{-1} \right) - 1}{2 \left( \frac{3}{\pi} \hat{i}_{123} I_{dc}^{-1} \right) - 1} \quad (\text{at } D_{sh} = 0) \quad (6)$$

The design of the output filter capacitors is relied on (2), where  $Q_f$  is varying only with the shunt capacitance  $C_f$ , keeping in mind that the voltage across this shunt filter is maintained by the AC grid. Figure 3 demonstrates the relation of  $I_{L1}$ ,  $i_f$  and  $D_{op}$  versus the shunt filter reactive power at 1.0 pu output real power and buck operation mode. Figure 4 shows the relation of the same variables as in Fig.3 but with changing the output power at 0.05 pu shunt filter reactive power.

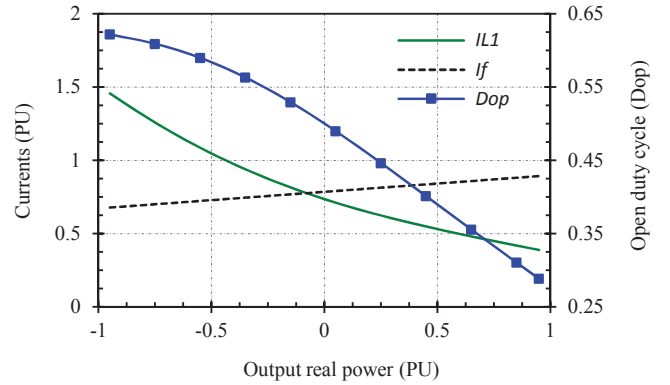


Fig. 3. Open-state duty cycle and circuit loop currents versus shunt filter reactive power ( $P_o = 1.0$  pu,  $V_{in} = 3$  kV,  $v_{o,L-L} = 2.5$  kV,rms and unity output power factor).

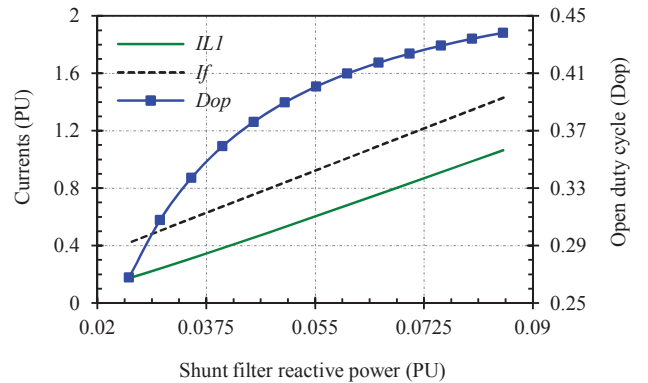


Fig. 4. Open-state duty cycle and circuit loop currents versus output real power ( $Q_f = 0.05$  pu,  $V_{in} = 3$  kV,  $v_{o,L-L} = 2.5$  kV,rms and unity output power factor).

The relations shown in Fig. 3 and Fig. 4 are obtained in per unit values, based on the rated power and voltage of the designed system, to be scalable for any power inverter size.

### III. SYSTEM CONFIGURATION

Figure 5 shows the single line diagram of the power system that analyzed in this study. The solar farm is connected to a weak distribution power system through a sub-transmission feeder and power transformer. Since the voltage magnitude and power angle at bus #1 are known, therefore, this power bus was considered the system swing bus. The power and voltage ratings of the solar farm are 10 MVA and 13.8 kV; respectively. Each solar array is interfaced with a DC-AC inverter and a step-up power transformer. The solar farm terminal bus is not facilitated with voltage regulation system which poses the challenge of unsettled voltage and frequency at the POI (bus #2). To solve this problem, step-change mechanical switched capacitors (MSCs) in range of ten kilovars are installed across bus #3. Moreover, a tap-changed (TC) power transformer is placed between the PV system and the POI bus to provide voltage support. It is worth mentioning that, the impact of these solutions are in discrete manner which does not satisfactorily regulate the intended voltage, and even poses other dynamic issues such as voltage flickers.

Therefore, the sub-transmission system that linked the PV system to the power grid is considered as the weakest part of the power system. It is concluded from [1] and [10] that connecting an oscillatory power source to a weak power sub-system can cause several significant problems. These problems includes power stability and the disability of injecting more active power. Moreover, the sensitive loads located nearby the weak portion of the system (e.g. induction motors), are exposed to harm or damage [21].

TABLE III. SPECIFICATION OF THE PV DISTRIBUTED GENERATION

Base power	10 MW
Module number per panel	4
Array terminal DC voltage	4.25 kV
Terminal rated power per array	0.59 kW
Power system base frequency	60 Hz
Switching frequency PV-VSI	3 kHz
Turns ratio of interface transformer	1:3.75

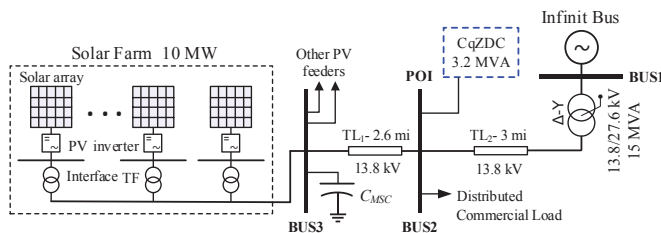


Fig. 5. Single line diagram of the studied power system.

### IV. CONTROL SYSTEM

The control system is divided into three sub-controllers; Supervisory control loop, inner control loop, and synchronization module.

#### A. Supervisory Control Loop

This control loop is responsible of generating the active and reactive power reference signals to conduct the desired operation mode as discussed in II. These reference values can be tracked by adjusting the  $d$  and  $q$  components of the converter output voltage, accordingly.

##### A.1 Active Power Smoothing Controller (APSC)

The first control mode of the supervisory control loop is the active power smoothing controller (APSC), which is utilized to smooth out the injected power by observing or suppling real power at the POI. In order to predict the pattern of the injected power trend, to be used in power smoothing process, the statistical linear regression analysis (LR) is used [22]. The main principle of the LR is the obtaining of future values of a time variant quantity using the pervious readings. This statistical tool can be utilized to trace the pattern of the SF injected power in order to determine the required behavior of the proposed versatile system. The main structure of the LR model is written as follows:

$$Y_{(k+1)} = \delta_{0,k} + \delta_{1,k} T_{k+1} + \mu \quad (7)$$

where  $Y$  is the predicted dependent variable that changes with time  $T$  and  $k$  is the current reading index.  $\mu$  is a random value that embedded to simulate the lost accuracy in the linearization process.  $\delta_0$  and  $\delta_1$  are the y-intercept and slope of  $k+1$  value, and they can be determined by:

$$\delta_1 = \left[ w \sum_x^k (Y_i T_i) - \sum_x^k Y_i \sum_x^k T_i \right] / \left[ w \sum_x^k (T_i)^2 - \left( \sum_x^k T_i \right)^2 \right] \quad (8)$$

$$\delta_0 = \left[ \sum_x^k (Y_i) - \delta_1 \sum_x^k (T_i) \right] / w \quad (9)$$

where  $w$  is the model window size (or the number of the used data in the regression process). Based on extensive simulation analysis, four previous readings as the regression window size ( $w=4$ ) with 2 minutes step time every 0.5 hour, yields a best fit to the SF injected power with a desired degree of smoothness.

##### A.2 Frequency and Voltage Deviation Controller (FDC and VDC)

On top of the fluctuated active power compensation, the frequency and voltage-droop ( $\omega V$ -droop) controller for grid-supporting converters are utilized to support the frequency and voltage magnitude at the POI [23]. The objective of  $\omega V$ -droop is to adjusting the inverter through output power based on power dispatch to suppress the voltage and frequency variations. By assuming a very small power angle (less than 0.1 rad), the converter output powers can be written as:

$$P_o X_p \approx V_{ab} V_s (\delta - \theta) \quad (10)$$

$$Q_o X_p \approx V_{ab} [V_{ab} - V_s] \quad (11)$$

where  $\delta$  and  $\theta$  are the power and power factor angle; respectively. It is concluded form (10) and (11) that the power angle  $\delta$  controls the inverter active power, while the magnitude

of the terminal voltage controls the inverter reactive power. Therefore, the grid bus frequency and voltage amplitude can be supported by adding the following active and reactive power references based on the ( $f$ - $P$ ) and ( $V$ - $Q$ ) droop characteristics (Fig. 6):

$$P_{f,ref} = P_n - P = K_d (f_n - f) \quad (12)$$

$$Q_{V,ref} = Q_n - Q = K_d (V_{s,n} - V_s) \quad (13)$$

where  $P_n$  and  $Q_n$  are the nominal real and reactive powers.  $V_{s,n}$  and  $f_n$  are the nominal terminal voltage and frequency.  $K_d$  and  $K_d$  are the proportional drooping frequency and voltage coefficients, as shown in Fig. 6.

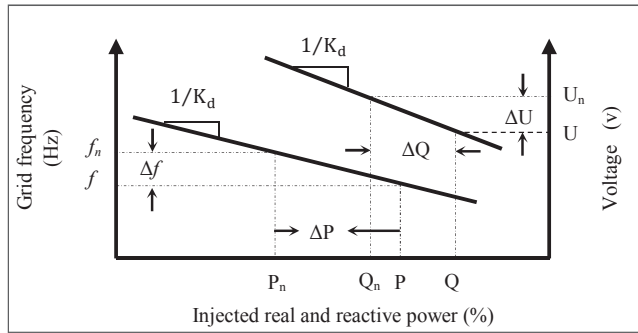


Fig. 6.  $\omega$ - $P$ ,  $U$ - $Q$  droop curves of  $\omega U$ -droop controller.

### A.3 Power Factor Correction Controller (PFCC)

High injected power factor can be maintained by controlling the current  $q$ -axis component, to make its summation with the SF current in-phase with the interface bus voltage. This control mode is activated when switch  $S_b$  is in position 2 (Fig. 8).

### A.4 Current Harmonic Filtering (CHF)

The THD of the injected current is improved by injecting the opposite phase shift of its high frequency harmonics, extracted using a high pass filter, to the inner loop current controller.

### B. Inner Control Loop

The inner control loop is designed to adjust the  $d$  and  $q$  components of the inverter terminal voltage in order to track the formulated power references. The voltage inner loop controller, with decoupled state variables, is constructed relying on [19]. The controller parameters are obtained via extensive simulations, for minimum possible steady state error. The state of charge (SOC) control circuit, utilized to control the battery current, is designed based on [12].

### C. synchronization module

In this controller part, the Clarke transformation formula is used to obtain the  $d$  and  $q$  components of a measured sinusoidal electrical quantity in  $abc$  reference frame. Moreover, the phase-locked-loop (PLL) is utilized in this control module to extract the system angular speed  $\omega_s$ . Fig. 8 shows the schematic of the control circuit in  $d$ - $q$  reference frame.

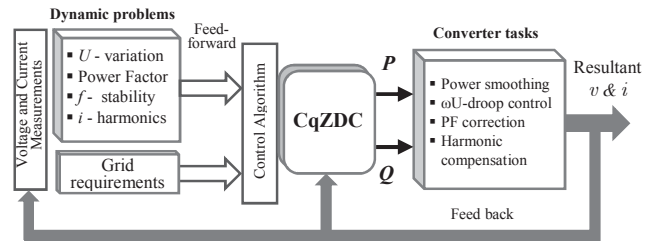


Fig. 7. Process flow of the proposed CqZDC system.

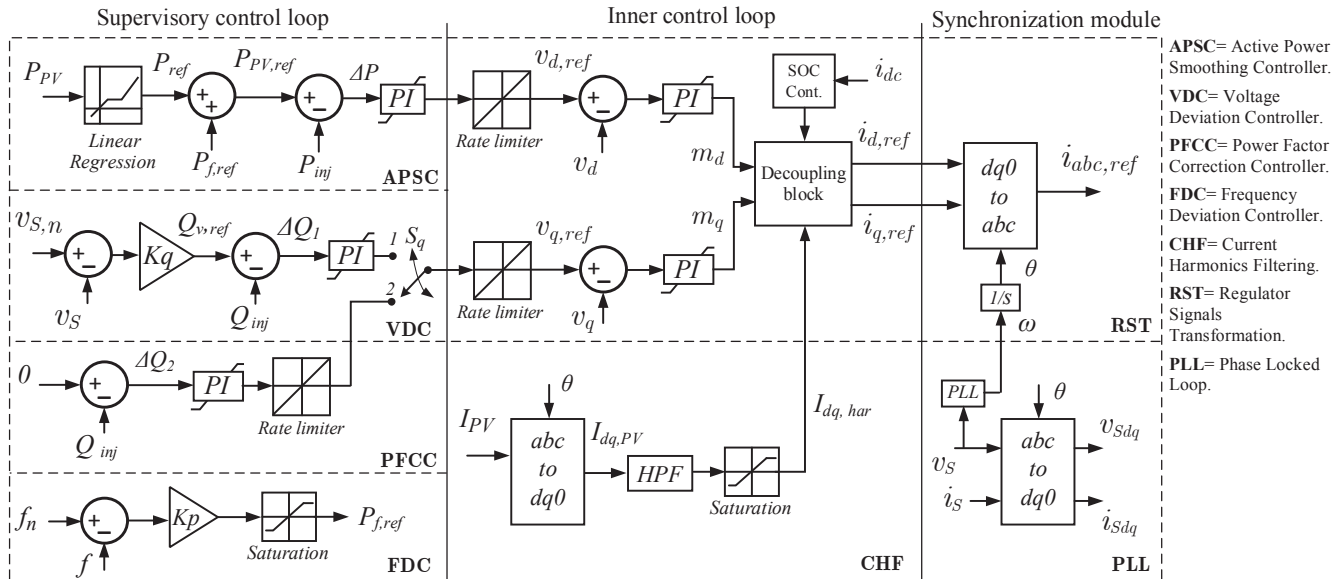


Fig. 8. Control circuit of the CqZDC system.

## V. SIMULATION ANALYSIS

### A. Power System Model Validation

The power system, as shown in Fig. 5, has been developed in Real Time Digital Simulator (RTDS), and a typical 10-hours operation (with 1-min sampling rate) was carefully selected to cover all possible injected power scenarios as shown in Fig. 10. And in order to address the power quality issues and the dynamic performance problems of the existed PV system, the real electrical data collected for the PV system were embedded to the simulation model. The grid loads are considered to be constant at 75% of the power transformer rating.

It is clearly seen from the dynamic performance in Fig. 10 that the SF injected power and voltage at the POI bus are aggressively fluctuating in different time period ranges. In addition, the uncontrolled reactive power at the POI bus causes a negative impact on the power factor of the SF injected power.

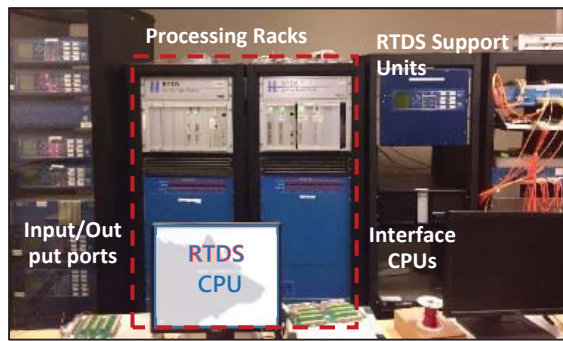


Fig. 9. RTDS simulation facility (for controller and system validation).

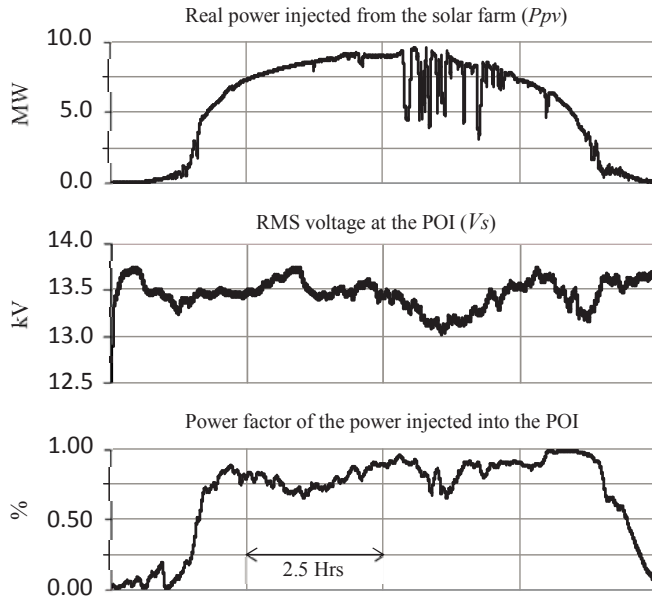


Fig. 10. Dynamic performance at the POI bus (without using the CqZDC).

### B. CqZDC Dynamic Response Test

The dynamic performance of the CqZDC device, when connected only to the power grid, is tested to show the device capability of controlling the active and reactive powers independently. Figure 11 illustrates the device performance

when the active and reactive power references are set at their maximum ratings with all possible scenarios. It is concluded that the CqZDC is able to regulate its output active and reactive powers independently in charging and discharging operation modes. Despite of that the power references were changing dramatically (step-change), the dynamic performance meets the grid requirements. The ESS terminal voltage is regulated by controlling the short-state and open-state duty cycles.

### C. CqZDC Dynamic Impact Evaluation

In this section, the CqZDC, is tested when it is connected in shunt with the SF system through the POI bus. Figures 11-17 demonstrate positive dynamic influence of the CqZDC. For example, in Fig. 12, the resultant injected PV power (blue line) has a smoother pattern than the original injected power (black line). In this figure, the worst case scenario of the solar radiation is illustrated. The smoothing process is conducted by activating the active power smoothing controller (APSC) mode, so that the power fluctuations is compensated by the ESS through the CqZDC device. This operation mode is conducted simultaneously with the PFCC mode, therefore, the CqZDC generates the required reactive power to reach zero reactive power injected to the POI bus, and therefore unity power factor as shown in Fig. 13.

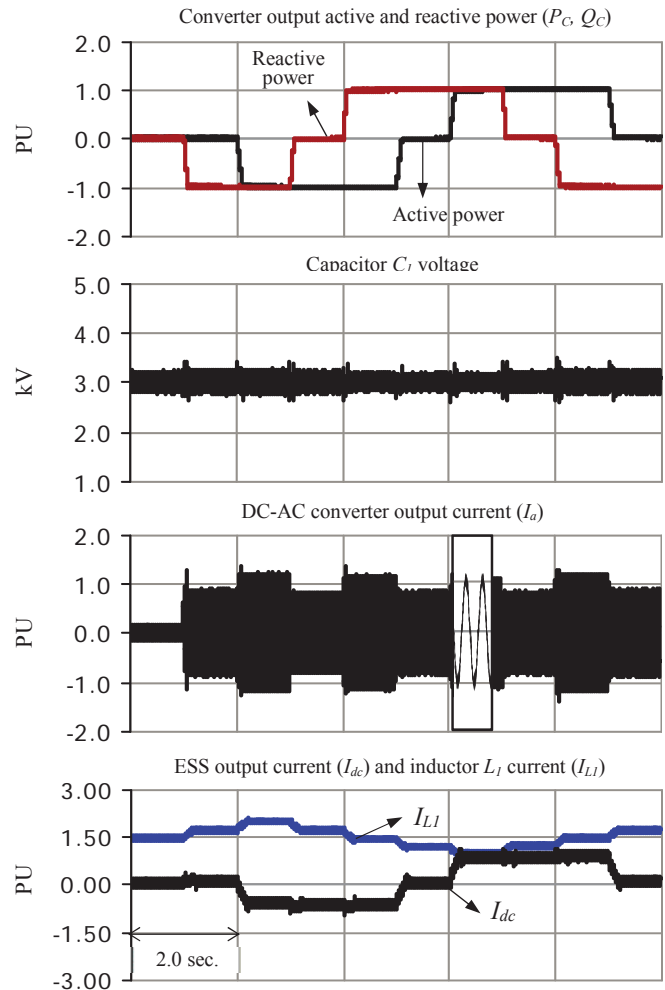


Fig. 11. Dynamic performance test of the CqZDC.

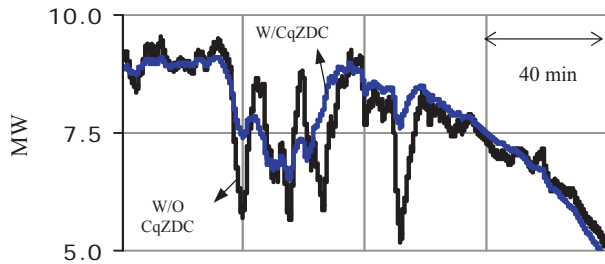


Fig. 12. Worst case injected real power into the POI bus ( $P_s$ ).

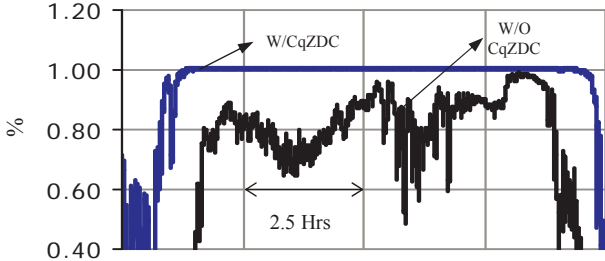


Fig. 13. Power factor of the power injected into the POI bus ( $P_s$ ) during the PFCC mode.

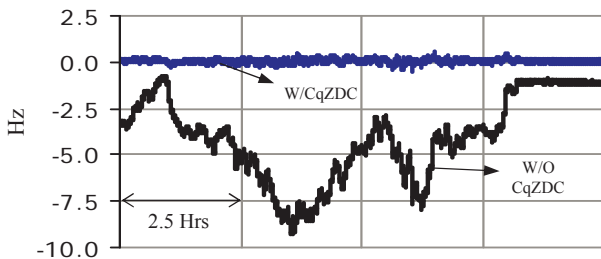


Fig. 14. Injected reactive power into the POI bus ( $Q_s$ ) during the PFCC mode.

It is concluded for the simulation results that the power factor can be maintained at unity value by adjusting the resultant injected reactive power accordingly via the CqZDC device (Fig. 14). The negative power factor value means that the CqZDC is operating during charging mode, i.e., the power is following from the power grid to the ESS system.

In addition, the POI voltage frequency response under sudden change ( $\pm 5$  MW) in the injected power with and without using the CqZDC is studied as shown in Fig. 15. According to the results, the frequency ROCOF is improved with using the CqZDC, while the frequency nadir was reduced from 60.9 Hz to 60.2 Hz. This reduction in frequency deviation is not resulted only by utilizing the FDC operation mode, but also the utilizing the APSC mode, where the sudden change in the injected power is mitigated. The dynamic impact of the CqZDC device is also validated during the VDC operation mode. POI bus voltage is suppressed by controlling the injected reactive power accordingly, as shown in Fig. 16. The steady state value of this voltage is also enhanced and kept at its rating voltage (13.5 kV), as set by the reference signal. In this case, the CqZDC device deliver the required Mvar to the POI, with opposite oscillation of the injected reactive power, in order to perform the desired terminal voltage. The peak oscillation of the POI bus voltage

has been suppressed from 3.8% to 0.72%, which validates the positive impact of the CqZDC on integration of the SF.

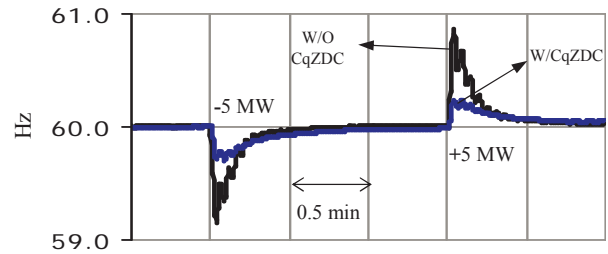


Fig. 15. Frequency response of THE POI bus voltage.

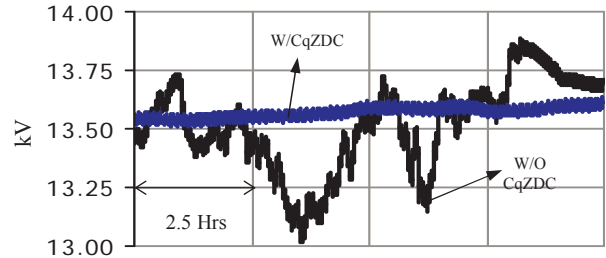


Fig. 16. Line voltage of POI bus ( $V_s$ ) during worst case.

Filtering out of harmonic contents in current and voltage waveforms at the POI bus (CHF mode) is also one of the operation modes of the CqZDC device. This operation modes is activated 2.5 hour after the initial time of the simulation to demonstrate the increased harmonic contents due the attachment of the CqZDC device. As shown in Fig. 17, the harmonics contents were reduced from 2.5%, 4.05% to 1.3%, 2.0% for the POI bus voltage and current, respectively. This reduction in harmonics verifies the feasibility of the CqZDC in enhancing the power quality of the power injected from renewable energy resources that interfaced by electronic based devices, which are considered as significant sources of current harmonics. This improving in the total harmonic distortion (THD) of the injected current and POI voltage also contributes in minimizing the power loss, therefore, increasing the SF sub-transmission efficiency.

The THD of the injected current and POI terminal voltage, become higher when the CqZDC device is attached to the system, and before applying the CHF mode, as shown in Fig. 17 (blue color). This slight increment in the THDs is due to the harmonic content in the output current of the CqZDC dc-ac power converter.

## VI. CONCLUSIONS

This paper proposes a current-fed quasi Z-source inverter, as an alternative topology for power conditioning systems (PCS) controlling a distribution renewable resource. This device can be connected at distribution system bus to perform several tasks, in order to enhance the power quality of an injected PV system, to meet the technical specifications required in grid codes. The detailed model and control algorithms of the proposed device are developed. The year-round simulation analysis, adopted by RTDS, indicate that the proposed solution

is feasible and has the ability to achieve the desired function with the size of 3.2 MVA. This study concluded that, the advantages of the CF-qZSI can be brought to the low rating energy storage systems based PCS applications.

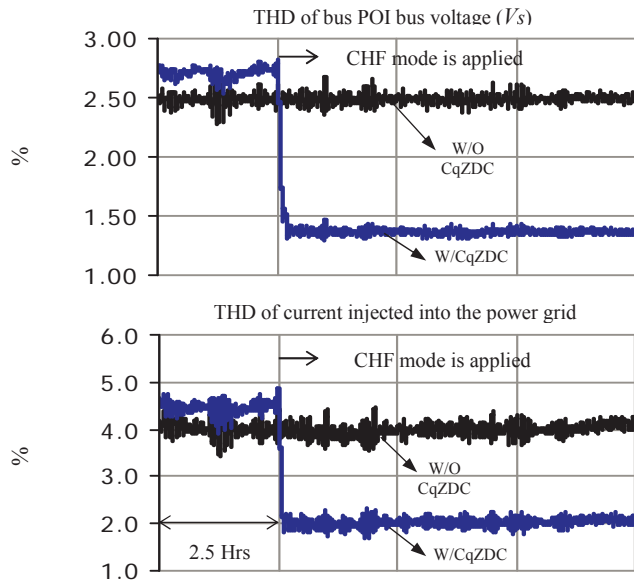


Fig. 17. Voltage and current THD at the POI bus.

#### APPENDIX

The truth Table for the switching pulse generator used for SVPWM to drive the CqZDC is shown in Table IV. The numbers “0” and “1” indicates the “OFF” and “ON” states of the inverter switches; respectively. X character means that the switch state does not matter (either ON or OFF).

TABLE IV  
TRUTH TABLE OF THE CQZDC SWITCHING PULSE GENERATOR

Top Switches			Bottom			State
S1	S3	S5	S2	S6	S4	
1	0	0	1	0	0	Active
1	0	0	0	1	0	Active
1	0	0	0	0	1	Short
0	1	0	1	0	0	Active
0	1	0	0	1	0	Short
0	1	0	0	0	1	Active
0	0	1	1	0	0	Short
0	0	1	0	1	0	Active
0	0	1	0	0	1	Active
0	0	0	X	X	X	Open
X	X	X	0	0	0	Open

#### ACKNOWLEDGMENT

This work was supported, in part, by the National Science Foundation. We would like to thank the FREEDM CENTER, North Carolina State University, Raleigh, NC. for providing the RTDS facility. Also, we would like to thank King Saud

University, Riyadh, Saudi Arabia and Saudi Arabian Cultural Mission, Fairfax, VA, 22031, for their support.

#### REFERENCES

- [1] Asrari, T. Wu and S. Lottifard, "The Impacts of Distributed Energy Sources on Distribution Network Reconfiguration," in *IEEE Transactions on Energy Conversion*, vol. 31, no. 2, pp. 606-613, 2016.
- [2] X. Liang, "Emerging Power Quality Challenges Due to Integration of Renewable Energy Sources," in *IEEE Transactions on Industry Applications*, vol. 53, no. 2, pp. 855-866, March-April 2017.
- [3] D. Remon, C. A. Cañizares and P. Rodriguez, "Impact of 100-MW-scale PV plants with synchronous power controllers on power system stability in northern Chile," in *IET Generation, Transmission & Distribution*, vol. 11, no. 11, pp. 2958-2964, 8 3 2017.
- [4] M. P. Musau, T. L. Chepkania, A. N. Odero and C. W. Wekesa, "Effects of renewable energy on frequency stability: A proposed case study of the Kenyan grid," *2017 IEEE PES PowerAfrica*, Accra, 2017, pp. 12-15.
- [5] M. Jafari, M. Popat and B. Wu, "Power Factor Control in a Wind Energy Conversion System via Synchronous Generator Excitation," in *Canadian Journal of Electrical and Computer Engineering*, vol. 37, no. 3, pp. 2014.
- [6] Z. H. Rather *et al.*, "Dynamic Reactive Power Compensation of Large-Scale Wind Integrated Power System," in *IEEE Transactions on Power Systems*, vol. 30, no. 5, pp. 2516-2526, Sept. 2015.
- [7] J. C. Das, "Application of STATCOM to an Industrial Distribution System Connected to a Weak Utility System," in *IEEE Transactions on Industry Applications*, vol. 52, no. 6, pp. 5345-5354, Nov.-Dec. 2016.
- [8] A. de la Villa Jaen, E. Acha and A. G. Exposito, "Voltage Source Converter Modeling for Power System State Estimation: STATCOM and VSC-HVDC," in *IEEE Transactions on Power Systems*, vol. 23, no. 4, pp. 1552-1559, Nov. 2008.
- [9] R. Sebastián, "Application of a battery energy storage for frequency regulation and peak shaving in a wind diesel power system," in *IET Generation, Transmission & Distribution*, vol. 10, pp. 764-770, 2 18 2016.
- [10] C. Han *et al.*, "STATCOM Impact Study on the Integration of a Large Wind Farm into a Weak Loop Power System," in *IEEE Transactions on Energy Conversion*, vol. 23, no. 1, pp. 226-233, March 2008.
- [11] L. J. Ontiveros, G. O. Suvire and P. E. Mercado, "Power conditioning system coupled with a flow battery for wind energy applications: modelling and control design," in *IET Renewable Power Generation*, vol. 11, no. 7, pp. 987-995, 6 7 2017.
- [12] Y. Yang, Q. Ye, L. J. Tung, M. Greenleaf and H. Li, "Integrated Size and Energy Management Design of Battery Storage to Enhance Grid Integration of Large Scale PV Power Plants," in *IEEE Transactions on Industrial Electronics*, vol. 65, no. 1, pp. 394-402, Jan. 2018.
- [13] J. Tant, F. Geth, D. Six, P. Tant and J. Driesen, "Multiobjective battery storage to improve PV integration in residential distribution grids," *2013 IEEE Power & Energy Society General Meeting*, Vancouver, BC, 2013.
- [14] K. H. Law, "An Effective Voltage Controller for Quasi Z-Source Inverter based STATCOM with Constant DC-Link Voltage," in *IEEE Transactions on Power Electronics*, vol. PP, no. 99, pp. 1-1.
- [15] Yang Ye, M. Kazerani and V. H. Quintana, "Current-source converter based STATCOM: modeling and control," in *IEEE Transactions on Power Delivery*, vol. 20, no. 2, pp. 795-800, April 2005.
- [16] S. Yang, F. Z. Peng, Q. Lei, R. Inoshita and Z. Qian, "Current-fed quasi-Z-source inverter with voltage buck-boost and regeneration capability," *2009 IEEE Energy Conversion Congress and Exposition*, San Jose, CA, 2009, pp. 3675-3682.
- [17] F. E. Alfaris and S. Bhattacharya, "A current-fed quasi Z-source inverter with SiC power modules for EV/HEV applications," *2017 IEEE Energy Conversion Congress and Exposition (ECCE)*, Cincinnati, OH, 2017, pp. 5445-5452.
- [18] Q. Lei, F. Z. Peng and B. Ge, "Transient modeling of current-fed quasi-Z-source inverter," *2011 IEEE Energy Conversion Congress and Exposition*, Phoenix, AZ, 2011, pp. 2283-2287.
- [19] M. Rashid, "Power Electronics Handbook." 4<sup>th</sup> edition, Butterworth-Heinemann, Oxford, United Kingdom, 2018.
- [20] F. Alfaris, A. Alzahrani and J. W. Kimball, "Stochastic model for PV sensor array data," *2014 International Conference on Renewable Energy Research and Application (ICRERA)*, Milwaukee, WI, 2014, pp. 798-803.
- [21] A. H. Bonnett, H. Glatt and S. Hauck, "Effect of Power Deviations on Squirrel-Cage Induction Motors: Addressing the Impact of Voltage and Frequency Variations," in *IEEE Industry Applications Magazine*, vol. 22, no. 6, pp. 39-47, Nov.-Dec. 2016.
- [22] X. Yan and X. Su, "Linear regression analysis. Theory and Computing." New York. World Scientific, 2009, pp. 201-204.
- [23] A. El Moubarek *et al.*, "Simulation of droop control strategy for parallel inverters in autonomous AC microgrids," *2016 8th (ICMIC)*, Algiers, 2016.